catalysts

MDPI

Article

Pore Structure Modification of the Mixed Metal Oxides Derived from Co-Al Layered Double Hydroxides and Catalytic Performance Enhancement for Aerobic Oxidation of Benzyl Alcohol

Qian Zhang [1], Xia Tan [1], Yinjie Hu [1], Haonan Cui [1], Xiao Lin [1,2], Fei Li [1,2], Huibin Lei [1,2] and Ou Zhuo [1,2,*]

[1] College of Chemistry and Chemical Engineering, Jishou University, Jishou 416000, China; zhangqq1108@126.com (Q.Z.)
[2] Hunan Province Key Laboratory of Mineral Cleaner Production and Green Functional Materials, Jishou University, Jishou 416000, China
* Correspondence: zhuoouhao@126.com

Abstract

The mixed metal oxides (MMOs) derived from layered double hydroxides (LDHs) are a typical class of porous materials and have attracted significant attention across various fields due to their high surface area, rich porous structures and various compositions. Regulating the pore structure of MMOs remains an urgent need because of the growing demand for numerous applications including adsorption, catalysis, and energy conversion. Controlling the lateral size of the lamellar crystals in the Co–Al LDH precursor allowed us to engineer the pore structure of Co–Al MMO, an architecture formed by the stacking of these lamellar flakes. The pore size distribution of the Co–Al MMO has been adjusted in the range from several nanometer to hundreds of nanometers. The sample with the optimized pore sizes exhibited a much higher catalytic reaction rate in the aerobic oxidation reaction of benzyl alcohol, about 4.2 times that of the control sample. Further research demonstrated that the high activity was favored by the improved mass transfer rate in the optimized pore architecture. Moreover, sodium silicate was employed as a cross-linking agent to enhance the cohesion within the secondary particles, which consist of stacked lamellar flakes. The resulting silicate-modified Co–Al MMO demonstrated significantly improved catalytic durability, maintaining stable performance over five consecutive reuse cycles—the performance that substantially exceeded that of its un-modified counterpart.

Keywords: layered double hydroxide; pore structure; pore modification; catalytic oxidation

check for updates

Academic Editors: Mario J. Muñoz-Batista and Akira Otsuki

Received: 8 September 2025
Revised: 19 October 2025
Accepted: 20 October 2025
Published: 22 October 2025

Citation: Zhang, Q.; Tan, X.; Hu, Y.; Cui, H.; Lin, X.; Li, F.; Lei, H.; Zhuo, O. Pore Structure Modification of the Mixed Metal Oxides Derived from Co-Al Layered Double Hydroxides and Catalytic Performance Enhancement for Aerobic Oxidation of Benzyl Alcohol. *Catalysts* **2025**, *15*, 1002. https://doi.org/10.3390/catal15111002

Copyright: © 2025 by the authors. Licensee MDPI, Basel, Switzerland. This article is an open access article distributed under the terms and conditions of the Creative Commons Attribution (CC BY) license (https://creativecommons.org/licenses/by/4.0/).

1. Introduction

The mixed metal oxides (MMOs), derived from the thermal decomposition of layered double hydroxides (LDHs), have attracted significant attention across various fields, such as catalysis [1–3], wastewater decontamination [4], electrode materials [5,6], and drug delivery [7,8]. MMOs usually present a nano-lamellar morphology with features of their high surface area, rich pores, and various compositions [2,9,10]. The nano-lamellar flakes of MMOs are constructed by stacking metal oxide nano-particles with a planar shape, which inherits the two-dimensional structure of LDH precursors [11,12]. The stacking of metal oxide nano-particles within the nano-lamellar flake generates numerous micropores and mesopores, while the subsequent stacking of lamellar flakes usually produces

a large amount of mesopores and macropores [13,14]. These hierarchical pores of MMO interconnect with each other and provide a large accessibility surface area and abundant tunnels for mass transfer, supplying excellent conditions to serve as porous function materials [15,16]. The fine tuning of MMO porosity is essential for achieving enhanced application performances [17–19].

The primitive strategy for tuning MMO porosity involves modifying the morphology, crystal size, and decomposition conditions of LDH precursors during the preparation period [18,20,21]. Jung et al. prepared a series of Mg–Al MMO samples with varying pore size distributions using different synthesis methods, which also exhibit different morphologies and particle sizes [22]. By adopting Pluronic F127 as a soft template, mesoporous Ni–Al MMO and Mg–Al MMO samples were successfully synthesized and exhibited excellent catalytic activity in the Knoevenagel condensation [15,23]. The study showed that the decomposition temperature of Ni–Al LDH precursors played a significant role in the pore size distribution of Ni–Al MMO [15]. Moreover, the pore sizes of mesoporous Mg–Al MMO were tuned by varying the concentrations of tris(hydroxymethyl) aminomethane, since the growth of Mg–Al LDH crystals could be effectively suppressed by this additive [23]. Guo et al. have also reported that the pore sizes of mesoporous Mg–Al MMO could be tailored by tuning sodium tartrate dosages in the co-precipitation process [24].

In addition, some specific treatment techniques have been applied to control the aggregation of LDH's lamellar flakes, allowing them to tune MMO's textural properties. The drying process can substantially influence the stacking structure of s MMO and its precursors (LDH) [20]. Freeze-drying and supercritical drying methods have been reported to successfully achieve higher porosity and/or tunable pore sizes for MMOs [20]. Controlling the reassembly of exfoliated LDH nanosheets has been extensively investigated as an effective way to modify the textural porosity of MMOs, which usually endues the MMO with ultrahigh surface areas and large pore volumes [20,25–27].

Despite the advances in regulating MMO pore structure described above, the tunable range of pore sizes remains too narrow to meet the demands, and the required procedures are often complex. Fine tuning MMO porosity remains an urgent need due to the growing demand for various applications including adsorption, catalysis, and energy conversion [17,20]. In this study, by controlling the lateral size of the lamellar crystals in the Co–Al LDH precursor, we successfully modulated the textual pore structure of the resulting Co–Al mixed metal oxide (MMO), which is composed of stacked lamellar flakes. This modification enabled the broad tuning of the pore size distribution in the Co–Al MMO. The optimized sample exhibited a significantly higher catalytic reaction rate in the aerobic oxidation of benzyl alcohol (BA), attributable to an enhanced mass transfer rate. Furthermore, sodium silicate was introduced as a cross-linking agent to strengthen the cohesion within the secondary particles composed of stacked lamellar flakes (Figure S1). The silicate-modified Co–Al MMO demonstrated markedly improved catalytic durability, maintaining stable performance over five consecutive reuse cycles—substantially outperforming its unmodified counterpart.

2. Results and Discussion

All Co–Al LDH samples were prepared by a modified coprecipitation method similar to our earlier reports [11,28]. The coprecipitation process was implemented by simultaneously pumping the salt solution and the alkaline solution into the $NaHCO_3$ solution at the same flow rate. A series of Co–Al LDH samples were synthesized by changing the pumping flow rate of the precursor solutions, named as CoAl-LDH-*x*, in which the *x* symbol represents the precursor addition rate ($mL \cdot min^{-1}$). The calcined CoAl-LDH-*x* sample was correspondingly labeled as CoAl-MMO-*x*.

The powder X-ray diffraction (XRD) patterns of the Co–Al LDH and Co–Al MMO samples are shown in Figures 1a and S2, respectively. All the Co–Al LDH samples displayed a variety of distinct diffraction peaks at 2θ values of 11.4°, 23.1°, 34.6°, 38.9°, 46.2°, 59.9°, and 61.2°, corresponding to the (003), (006), (012), (015), (018), (110), and (113) facets of the LDH (JCPDS #51-0045) [27,29]. No diffraction signals corresponding to phases other than Co–Al LDH were observed in Figure 1a, indicating that all samples consist of a high-purity Co–Al LDH phase. Additionally, the diffraction intensity, especially for (003) facets, obviously decreases with increasing pumping flow rates of precursor solutions during coprecipitation. This phenomenon should be closely correlated with the essential roles of the supersaturation level of ionic precursor (metal cations and OH^-) during the LDH crystal formation [30,31]. Specifically, the high precursor addition rate induces a high supersaturation level in the coprecipitation solution, thereby kinetically favoring the formation of LDH crystals with diminished crystallinity and particle sizes [30].

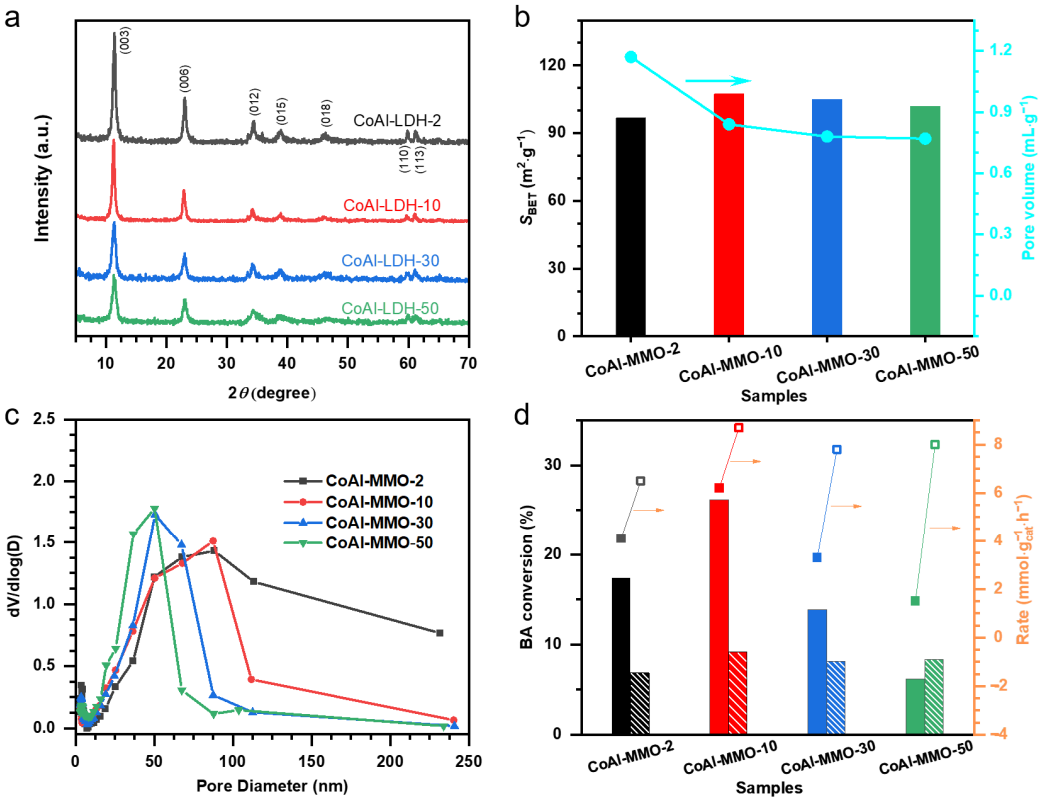


Figure 1. The characterization and catalytic performance of the Co–Al MMO samples and their LDH precursors. (**a**) XRD patterns of the Co–Al LDH samples; (**b**) S_{BET} and pore volumes of the Co–Al MMO samples; (**c**) pore size distributions of the Co–Al MMO samples; and (**d**) the conversions and reaction rates for aerobic BA oxidation in low (left column and left dot of each sample) and high (right column and left dot of each sample) BA concentrations. The corresponding N_2 adsorption/desorption isotherms data for (**b**,**c**) are provide in Figure S4 in the Supporting Information. Catalytic reaction conditions for low concentrations: 20 mL N,N-dimethylformamide (DMF), 1.00 mL BA, 100 mg catalyst, 1.0 MPa O_2 pressure, 120 °C, 4 h; all conditions for high concentrations are identical to that of low concentration except for increasing the BA dosage to 4.00 mL.

The Co–Al MMO was obtained via thermal decomposition of Co–Al LDHs through calcination in a tube furnace, with more details provided in the Experimental Section (Section 3) below. The XRD patterns show that Co_3O_4 is the predominant crystalline phase in all the Co–Al MMO samples (Figure S2). No characteristic diffraction peaks were detected for Al-containing oxides or other phases (Figure S2), which suggests the amorphous nature of the Al species or particles with dimensions beyond the XRD detection

threshold. The specific surface areas (S_{BET}) of the Co–Al MMO samples are not much different, all close to 100 $m^2 \cdot g^{-1}$ (Figure 1b). Notably, the pore volumes decreased from 1.17 to 0.77 $mL \cdot g^{-1}$ with increasing precursor flow rate from 2 to 50 $mL \cdot min^{-1}$ (Figure 1b), indicating significant differences in pore structure.

The pore size distributions of the Co–Al MMO samples are presented in Figure 1c. The CoAl-MMO-2 sample exhibits a broad pore size distribution spanning from several nanometers to several hundred nanometers. The CoAl-MMO-10 sample displays a distribution predominantly ranging from several nanometers to approximately 100 nm, with an increase in mesopore content (2–50 nm) and a significant decrease in macropore content relative to the CoAl-MMO-2 sample. The pore sizes of the CoAl-MMO-30 and CoAl-MMO-50 samples show a continuous decreasing trend, demonstrating an inverse correlation with the precursor addition rate. Interestingly, the CoAl-MMO-50 sample exhibits predominantly mesoporous structures, which suggests a viable synthesis pathway for mesoporous materials.

To investigate the influence of pore size distribution on mass transfer, we employed the aerobic oxidation of BA as a probe reaction and measured the catalytic reaction rates of all samples at a low conversion. As shown in Figure 1d, the CoAl-MMO-10 sample displayed the highest BA conversion, about 4.2 times higher than that of the CoAl-MMO-50 sample. Considering that the two catalysts exhibited a nearly identical composition, structure, S_{BET}, and synthesis method, yet exhibited significant differences in catalytic reaction rate, we hypothesized that the reaction rates were determined by mass transfer rate, rather than intrinsic catalytic activity. To verify this hypothesis, we increased the initial BA concentration fourfold, thereby increasing the mass transfer rate and minimizing the influence of mass transfer on the reaction rates. The experimental results showed that the reaction rates of the two catalysts became relatively close (8.7 and 8.0 $mmol \cdot g_{cat}^{-1} \cdot h^{-1}$) (Figure 1d). This indicates that BA mass transfer is the limiting factor for the reaction rate at low BA concentrations (the former reaction conditions). Furthermore, after grinding the CoAl-MMO-50 sample to the secondary particle size smaller than 25 μm, the reaction rate incresed to about 13 $mmol \cdot g_{cat}^{-1} \cdot h^{-1}$, which should be close to the intrinsic catalytic activity (Figure S3a). Additionally, the reduced O_2 pressure condition also led to approximate reaction rates between the two catalysts, which was accompanied by much slower reaction rates and therefore diminished the requirements of mass transfer (Figure S3b). The catalytic performances of other catalysts displayed similar change trends (Figures 1d and S3). These results confirm that BA mass transfer is a decisive factor for the reaction rate. A fully quantitative analysis of diffusion limitations could further substantiate this conclusion and benefit catalyst engineering. However, we reserve such an analysis for future work to maintain a focus on modifying the pore structure of the Co-Al MMO. In brief, the CoAl-MMO-10 sample exhibited the highest catalytic activity mainly due to its higher mass transfer rate, which should be attributed to the optimized pore structure. In contrast, the CoAl-MMO-2 sample presented lower catalytic activity, owing to its underdeveloped pore structure, which featured the least amount of mesopores (Figure 1c).

Figure 2 presents the scanning electron microscope (SEM) and transmission electron microscope (TEM) images characterizing the morphology of the Co–Al MMO samples. As shown in Figure 2a–d, all the Co–Al MMO samples exhibit a well-defined porous structure consisting of stacked lamellar flakes, which is typical feature of LDH-derived MMO materials. Figure 2a–d demonstrate a significant progressive reduction in stacking pore dimensions, consistent with BJH analysis results (Figure 1c). Moreover, the mean lateral sizes of the lamellar flakes gradually decrease from 336 to 64 nm when increasing the precursor flow rate from 2 to 50 $mL \cdot min^{-1}$ during coprecipitation (Figure 2e–h). This illustrates that the lateral crystal dimensions of LDH flakes are inversely related with the

precursor feed rates, since the lamellar morphology of MMO inherits the LDH crystal flakes. Additionally, the TEM images also show similar change trends (Figure 2i–l). In brief, the lateral sizes of the lamellar MMO flakes are controllable through tuning precursor addition rates in coprecipitation and thereby achieve regulation of the pore size distribution.

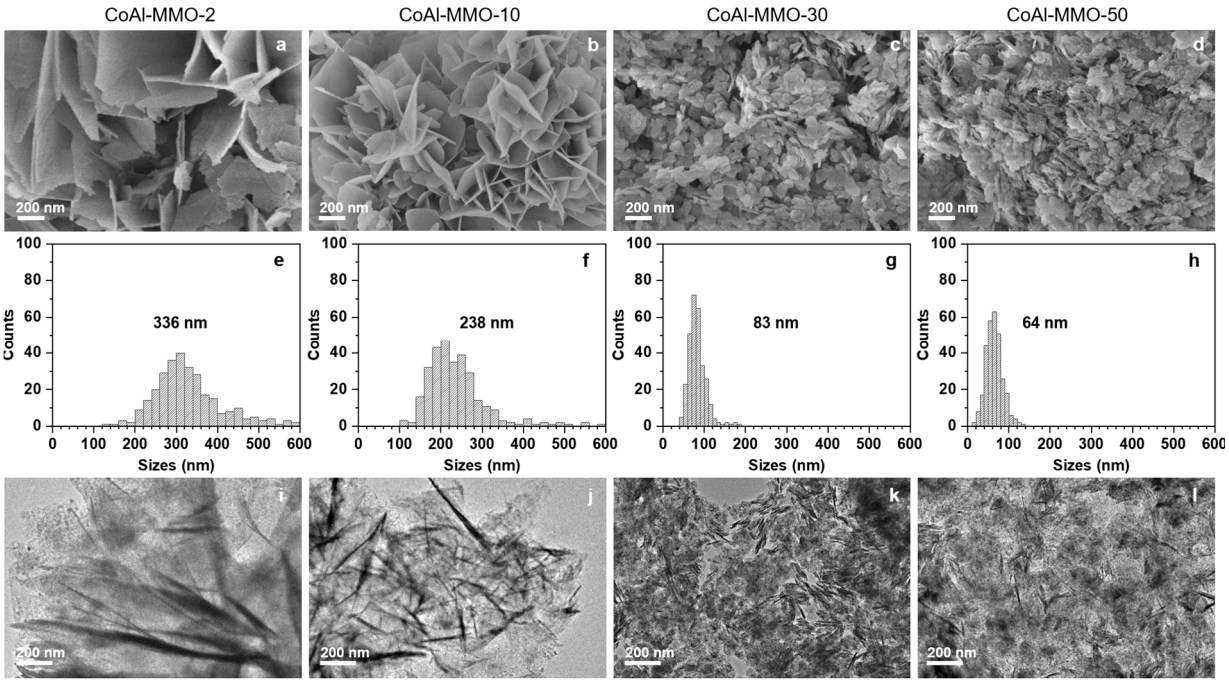


Figure 2. Microscopic characterization of the Co–Al MMO samples. (**a**–**d**) SEM images, (**e**–**h**) lateral size histograms of lamellar flakes, and (**i**–**l**) TEM images of the CoAl-MMO-2, CoAl-MMO-10, CoAl-MMO-30, and CoAl-MMO-50 samples, respectively. The lateral sizes of the MMO lamellae were determined by measuring 300 particles from the SEM images.

The regulation of the pore distribution has substantially enhanced the mass transfer rate of the Co–Al MMO material and consequently improved the catalytic reaction rate in the aerobic oxidation of BA. However, the lamellar flakes of MMOs tend to delaminate from the secondary particles under vigorous stirring in the liquid phase [2,20,25]—a condition routinely indispensable in gas–liquid-solid catalysis systems for enhancing gas–liquid mass transfer rates. This structural instability not only triggers catalytic deactivation but also complicates post-reaction filtration separation [32]. We tried to use sodium silicate, which is widely employed as a binder [33,34], to improve the stacking cohesion of lamellar flakes, thereby enhancing the structural stability of the secondary particles of the Co–Al MMO.

The silicate-modified Co–Al MMO samples were synthesized by washing the LDH precursors with a sodium silicate solution of different concentrations after deionized water washing, without changing the synthesis method and other conditions mentioned above (details seen in Experimental Section (Section 3)). Four modified samples were prepared using sodium silicate solutions at different concentrations (0.02, 0.04, 0.06, and 0.08 mol·L^{-1}), designated as CoAl-LDH-Sx (x = 1–4), where "S" denotes sodium silicate modification and "x" indicates the relative concentration gradient. The XRD peak intensities of the silicate-modified Co-Al LDH samples gradually decreased with increasing sodium silicate solution concentration, although no distinct silica-containing crystalline phase was detected (Figures 3a and S5). The energy dispersive X-ray spectroscopy (EDX) mapping data confirms the successful incorporation of silica-species into the MMO sample (Figure S6).

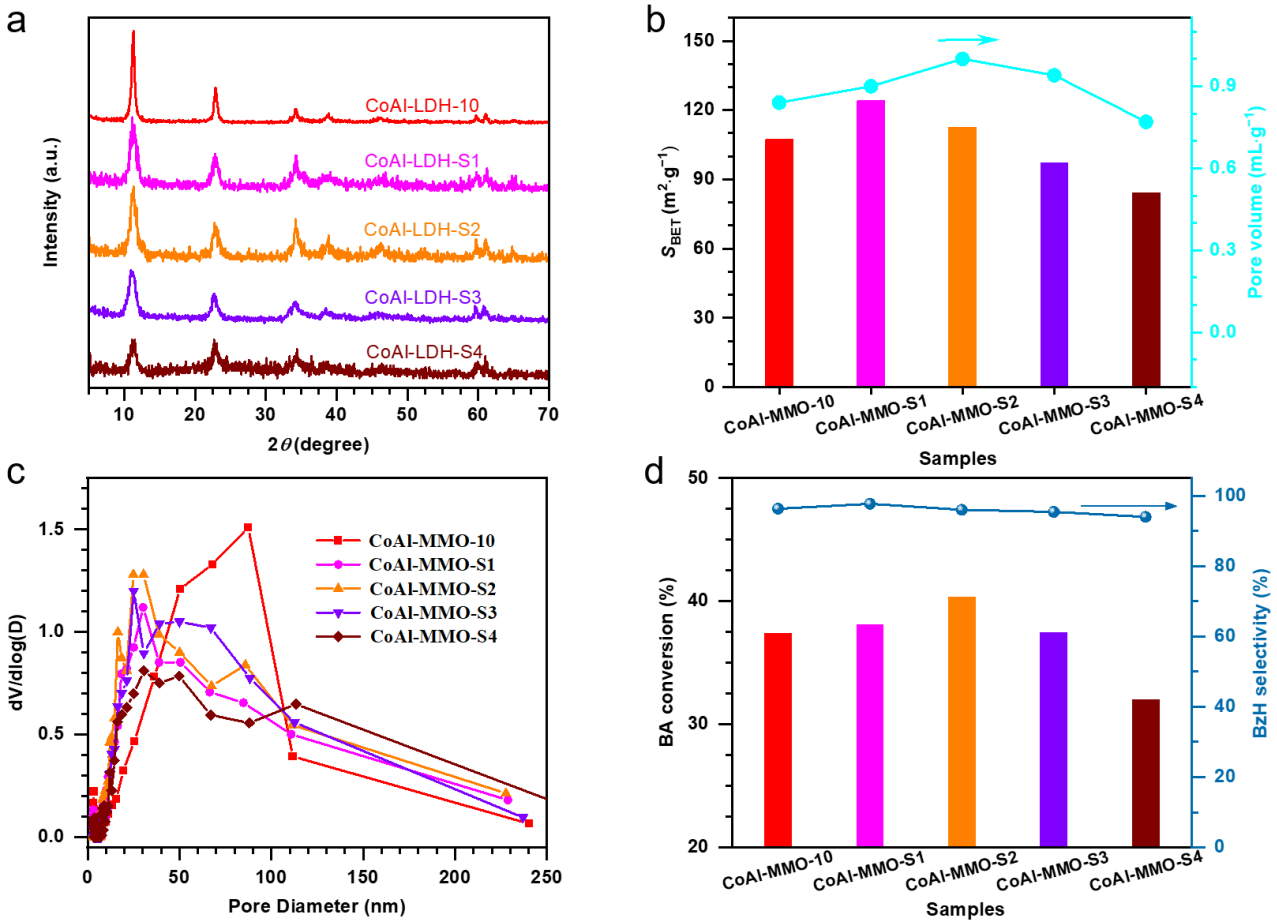


Figure 3. The characterization and catalytic performances of the silicate-modified Co–Al MMO samples and their LDH precursors. (**a**) XRD patterns of the silicate-modified Co–Al LDH samples; (**b**) S_{BET} and pore volumes of the silicate-modified Co–Al MMO samples; (**c**) pore size distributions of the silicate-modified Co–Al MMO samples; (**d**) the conversions and benzaldehyde (BzH) selectivity for aerobic oxidation of BA. The corresponding N_2 adsorption/desorption isotherms data for (**b**,**c**) are provide in Figure S4 in the Supporting Information. Catalytic reaction conditions: 20 mL N,N-dimethylformamide (DMF), 0.50 mL BA, 100 mg catalyst, 0.2 MPa O_2 pressure, 130 °C, 12 h. The XRD pattern, S_{BET}, pore volume, pore size distribution, BA conversion, and BzH selectivity for the CoAl-MMO-10 sample from Figure 1 are replotted in Figure 3a, b, c, and d for comparison, respectively.

The S_{BET} and pore volumes of the silicate-modified Co–Al MMO samples showed a concentration-dependent correlation with the sodium silicate solution. Samples with lower concentrations (CoAl-MMO-S1 and CoAl-MMO-S2) exhibited higher S_{BET} and pore volumes than the control sample (CoAl-MMO-10), whereas higher-concentration samples (CoAl-MMO-S3 and CoAl-MMO-S4) displayed considerably reduced values (Figure 3b). Furthermore, silicate modification obviously increased mesopore density while reducing the macropore content compared to the control sample (Figure 3c). Except for the CoAl-MMO-S4 sample, the silicate-modified samples exhibited relatively high catalytic reaction rates as compared with the un-modified control sample (CoAl-MMO-10) in aerobic BA oxidation (Figure 3d). Notably, the CoAl-MMO-S2 catalyst, with the highest mesopore content (10–40 nm), achieved the highest catalytic reaction rate (Figure 3c,d). Given that the previous results showed that mass transfer is the determining factor for the catalytic reaction rate, these results illustrate that mesopores significantly influence mass transfer. In other words, the optimized hierarchical pore structure (including mesopores and macropores) of the MMO is beneficial for improving the mass transfer rate and reaction rate. Moreover, the CoAl-MMO-S2 catalyst also demonstrated well catalytic performance for other substrates

(Table S1). Additionally, the CoAl-MMO-S4 sample exhibited the lowest catalytic reaction rate, which was primarily due to its reduced pore volume and S_{BET} (Figure 3d).

Figure 4 illustrates the microscopic structure and morphology of the silicate-modified CoAl-MMO-S2 sample. The SEM (Figure 4a), TEM (Figure 4b), and high-angle annular dark-field TEM (HAADF-TEM) (Figure 4c) images clearly demonstrate a well-defined porous structure, with no obvious differences observed relative to the control sample (CoAl-MMO-10). The nano-lamellar flakes of the MMO were clearly observed in the images (Figure 4a–d), which are composed of randomly stacked Co_3O_4/Al_2O_3 nano-particles with a planar shape (Figure 4d,e). The EDX mapping images (Figure 4g–k) of the CoAl-MMO-S2 sample reveal that the distribution of Co, Al, and Si elements well match with the morphology observed by the corresponding HAADF-TEM image (Figure 4f). This shows that the various elements in the sample are all uniformly dispersed, especially for silicon species.

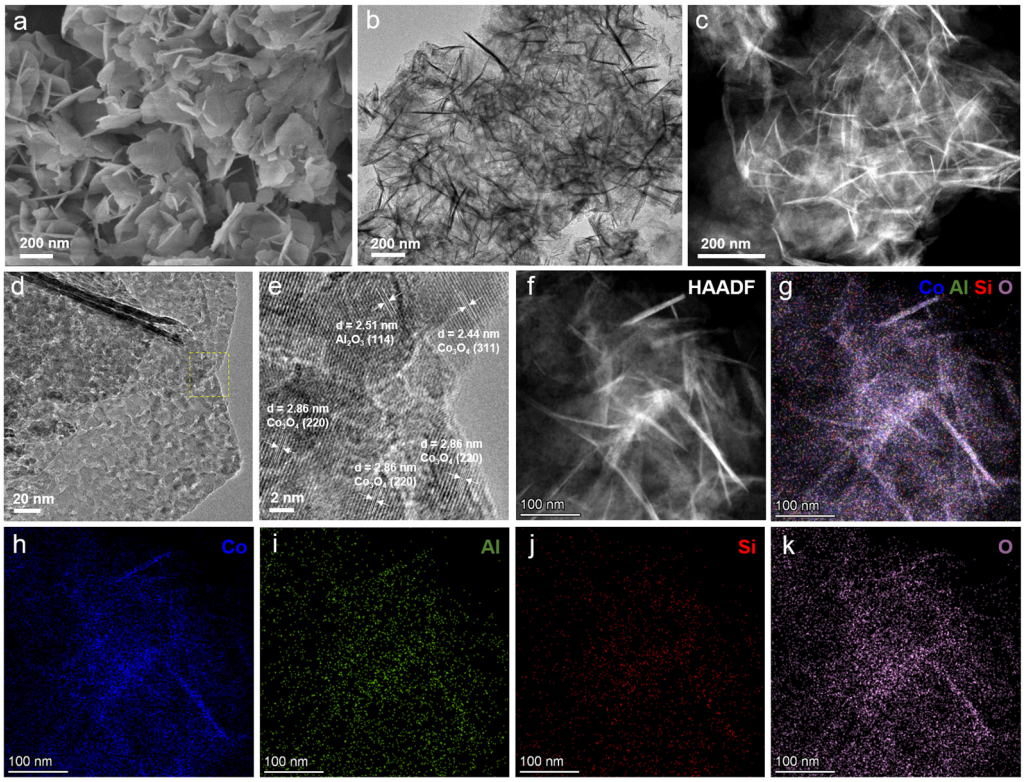


Figure 4. Microscopic characterization of the CoAl-MMO-S2 sample. (**a**) SEM image, (**b**) TEM image, (**c**) HAADF-TEM image, (**d**) TEM image, (**e**) high-resolution TEM image (the area marked by the yellow box in **d**), and (**f**–**k**) HAADF-TEM and corresponding EDX mapping images of the CoAl-MMO-S2 sample.

To examine the impact of silicate modification on the structural stability of the Co–Al MMO, the catalytic performances of the un-modified and modified samples were evaluated over five consecutive reuse cycles. The results demonstrate divergent evolution trends: the modified sample (CoAl-MMO-S2) exhibited sustained BA conversion efficiency, in contrast to the progressive degradation observed in the un-modified counterpart (CoAl-MMO-10) (Figure 5a). To investigate the mechanism of catalytic stability improvement by silicate modification, the evolution trend of secondary particle sizes over cycles for the two samples was measured by the laser diffraction method. Notably, significant changes in the secondary particle sizes were detected for both samples after use (Figure 5b), indicating the exfoliation of lamellar flakes from the secondary particles. A large number of isolated lamellar flakes were observed in the TEM and SEM images of the used un-modified sample

(Figures 5c and S7a), confirming the lamellar delamination from the secondary particles (Figure 5c,d). Furthermore, particle size distribution analysis revealed a more pronounced reduction in the un-modified sample (from 1.5 to 1.8 μm to 0.8–1.1 μm after a single use) compared to the silicate-modified counterpart (from 1.4 to 2.0 μm to 1.0–1.7 μm). These results demonstrate that silicate modification significantly enhances the mechanical stability of the MMO's structure, thereby suppressing its deterioration under vigorous stirring in the liquid phase under the catalytic reaction condition. Moreover, the TEM and SEM images also suggest that the modified sample has better structural stability, based on substantially fewer delaminated flakes in the used sample (Figures 5c,d and S7). The enhanced structural stability endowed the modified MMO with stable catalytic activity in the reaction (Figure 5a). Nevertheless, after five reaction cycles, the secondary particle size of the modified sample has significantly reduced, showing only a marginal improvement compared to the un-modified sample (Figure 5b). This strategy still cannot meet the needs of practical applications, so further studies are required.

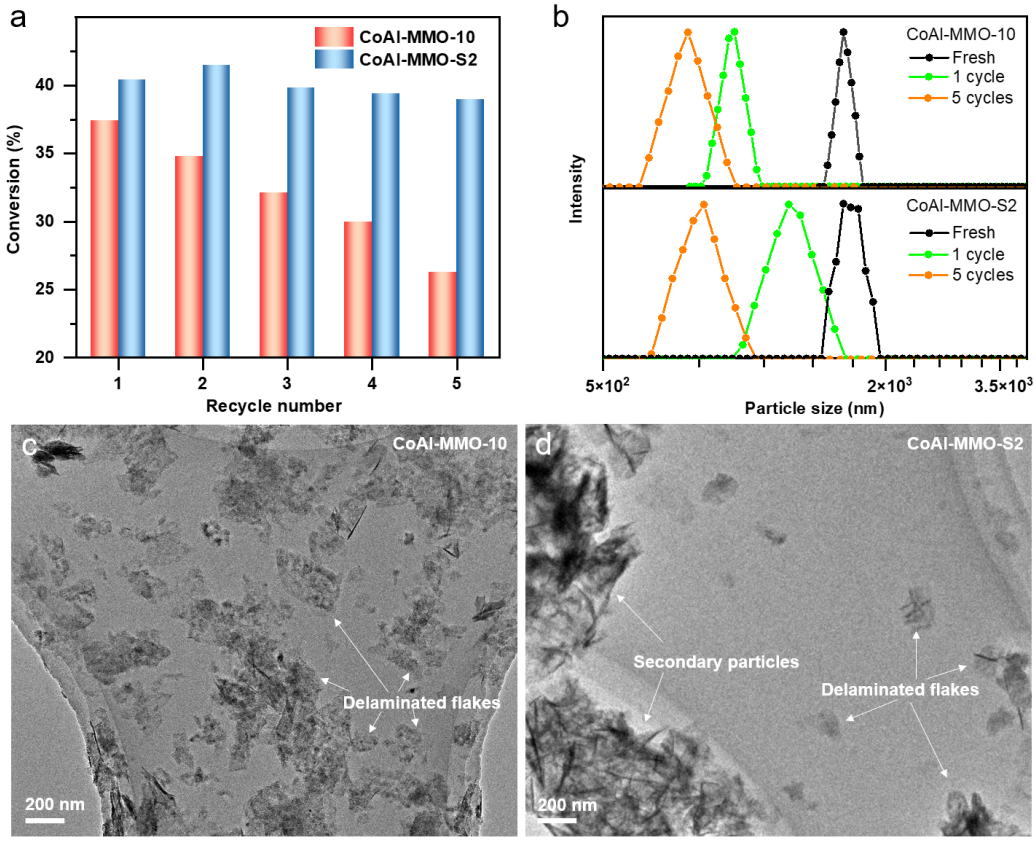


Figure 5. The BA conversion and structural characterization of the un-modified and silicate-modified Co–Al MMO samples over five consecutive reuse cycles. (**a**) BA conversions; (**b**) particle size distributions of secondary particles measured by laser diffraction method; (**c**,**d**) TEM images of the CoAl-MMO-10 (**c**) and CoAl-MMO-S2; and (**d**) samples after a single use, respectively.

3. Experimental Section

3.1. Preparation of Samples

All Co–Al LDH samples were prepared by a modified coprecipitation method, in which the operated processes were similar to our earlier reports [11,28]. Typically, the salt solution was prepared by dissolving a mixture of $Co(NO_3)_2$ and $Al(NO_3)_3$ (the total metal amount is 0.06 mol with Co/Al molar ratio of 75/25) in 120 mL of deionized water. The alkaline solution was obtained by dissolving 0.12 mol of NaOH in 120 mL of deionized water. Then, 0.018 mol of $NaHCO_3$ was dissolved in 150 mL of deionized water within a

three-necked flask. After the temperature increased to 80 °C, the salt solution and alkaline solution were simultaneously pumped into the flask (using two Series II pump from Lab Alliance, NY, USA) at the same flow rate of x mL/min (x = 2, 10, 30, or 50). The slurry was stirred gently at 80 °C for 10 h. The resulting precipitate was filtered, washed with deionized water, and dried at 80 °C for 10 h. The obtained Co–Al LDH sample was ground into a fine powder and labeled as CoAl-LDH-x. Each Co–Al LDH sample was calcined at 500 °C for 2 h in a tube furnace under air flow (500 mL·min^{-1}). After naturally cooling to an ambient temperature, the Co–Al MMO sample was obtained and named as CoAl-MMO-x.

The silicate-modified Co–Al LDH samples were synthesized under identical method and conditions, except for an additional rinsing step. Specifically, after washing with deionized water, the filter cake was washed once with 200 mL sodium silicate solution at a specified concentration (0.02, 0.04, 0.06, or 0.08 mol·L^{-1}) and then dried under the same conditions. The resulting four samples, prepared with these different concentrations, were designated as CoAl-LDH-Sx (x = 1–4).

3.2. Catalyst Characterization

XRD measurements were conducted on a TD-3500 X-ray diffractometer (Dandong Tongda Instrument Co., Dandong, China, $\lambda_{\mathrm{Cu\,K}a}$ = 0.15418 nm, 35 kV, and 25 mA). The N_2 adsorption/desorption isotherm data were recorded on a surface area and pore size analyzer of Nova 2000e (Quantachrome, Boynton Beach, FL, USA). All samples were degassed under vacuum at 200 °C for 12 h before measurement. The Brunauer–Emmett–Teller specific surface areas (S_{BET}) were calculated using adsorption branch data, and the Barrett–Joyner–Halenda (BJH) model was utilized to calculate pore size distributions. The pore volumes were determined from the last point of the adsorption branch data ($P/P_0 \approx 0.995$). TEM and high-resolution TEM images were obtained with a Talos F200S instrument operated at an accelerating voltage of 200 kV (Thermo Fisher, Waltham, MA, USA). HAADF-TEM and corresponding EDX mapping images were recorded on a SUPER X detector. SEM images were achieved on a Zeiss-Sigma 300 instrument at an accelerating voltage of 30 kV (Carl Zeiss Jena, Jena, TH, Germany). The particle sizes of Co–Al MMO's secondary particles were measured using a Nanobrook 90 Plus zeta potential and particle size analyzer (Brookhaven, NY, USA) with a detection mode covering particle sizes of 0.3–15 μm. Prior to testing, all samples were diluted with deionized water and dispersed via ultrasonication.

3.3. Catalytic Testing

The liquid-phase oxidation of BA was performed in a 60 mL stainless steel reactor. First, 100 mg catalyst, 0.50/1.00/4.00 mL BA, and 20 mL DMF were added to the reactor. Then, the reactor was sealed and purged with O_2 for several cycles to remove air. After the temperature of the reactor rose to the setting value (120 or 130 °C), the O_2 pressure was elevated to 0.2/1.0 MPa and the liquid mixture was stirred magnetically at 600 rpm. After 12 h of reaction, the reactor was cooled to room temperature naturally. The liquid mixture was filtrated in a glass funnel. The catalyst was subsequently washed with 5 mL ethanol and dried at 80 °C for 10 h for reuse. Finally, the filtrated liquid (1.00 mL of reaction products with 100 mg of biphenyl as internal standard) was analyzed by a gas chromatography system (Qiyang GC9860) equipped with a flame ionization detector and an AT-PONA capillary column (50 m × 0.20 mm, d_{f} = 0.5 μm). The error in repeated testing of catalytic performance is small (Table S2). The catalytic stability was evaluated over five reuse cycles of the spent catalyst, with all other operating procedures and conditions identical to those described above, except for the addition of a small amount of fresh catalyst to maintain a total catalyst mass of 100 mg.

4. Conclusions

The lateral size of the Co–Al LDH's lamellar flakes have been effectively regulated by modulating precursor addition rates during coprecipitation. This dimensional control enabled systematic modification of the textural pore structure of the derived Co–Al MMO, which is composed of lamellar flake stacking. The modification of pore size distribution significantly enhanced mass transfer efficiency, leading to a multi-fold increase in catalytic reaction rates for BA aerobic oxidation compared to control samples. To improve mechanical stability of the Co–Al MMO's structure, sodium silicate was employed as a cross-linking agent to reinforce cohesion within the secondary particles. The silicate-modified Co–Al MMO exhibited exceptional catalytic durability, maintaining activity stability over five consecutive reuse cycles—a performance markedly superior to the unmodified counterpart. This study presents a scalable methodology for tailoring the MMO pore structures, offering a viable pathway for the structural optimization in catalytic applications.

Supplementary Materials: The following supporting information can be downloaded at: https://www.mdpi.com/article/10.3390/catal15111002/s1, Figure S1: Schematic illustration of the proposed hierarchical structure of Co–Al MMO; Figure S2: The XRD patterns of the Co–Al MMO samples; Figure S3: The catalytic reaction results for aerobic BA oxidation under different reaction conditions; Figure S4: The N_2 adsorption/desorption isotherms data of the Co–Al MMO and silicate-modified Co–Al MMO samples; Figure S5: The XRD patterns of the silicate-modified Co–Al MMO samples; Figure S6: The EDX mapping results of the CoAl-MMO-S2 sample; Figure S7: SEM images of the CoAl-MMO-10 and CoAl-MMO-S2 samples after a single use; Table S1: Aerobic oxidation of various substrates using the CoAl-MMO-S2 sample; Table S2: Three repeat experiment results of the aerobic oxidation of BA.

Author Contributions: Conceptualization, O.Z., X.L., and F.L.; methodology, O.Z., X.L., and H.L.; synthesis and catalytic testing, Q.Z.; formal analysis, Q.Z., X.T., Y.H., and H.C.; data curation, Q.Z., X.T., and Y.H.; writing—original draft preparation, O.Z. and Q.Z.; writing—review and editing, O.Z., Q.Z., and X.L.; supervision, O.Z.; project administration, O.Z.; funding acquisition, O.Z., X.L., F.L., and H.L. All authors have read and agreed to the published version of the manuscript.

Funding: This work was supported by the National Natural Science Foundation of China (grant number 22368021) and the Hunan Provincial Natural Science Foundation of China (grant number 2023JJ40516, 2024JJ7401, and 2024JJ7417).

Data Availability Statement: The data presented in this study are available in the article.

Conflicts of Interest: The authors declare no conflicts of interest.

References

1. Jiang, S.; Zhang, M.; Xu, C.; Liu, G.; Zhang, K.; Zhang, Z.; Peng, H.-Q.; Liu, B.; Zhang, W. Recent Developments in Nickel-Based Layered Double Hydroxides for Photo(-/)electrocatalytic Water Oxidation. *ACS Nano* **2024**, *18*, 16413–16449. [CrossRef]
2. Xu, M.; Wei, M. Layered Double Hydroxide-Based Catalysts: Recent Advances in Preparation, Structure, and Applications. *Adv. Funct. Mater.* **2018**, *28*, 1802943. [CrossRef]
3. Li, S.; Wang, D.; Wu, X.; Chen, Y. Recent advance on VOCs oxidation over layered double hydroxides derived mixed metal oxides. *Chin. J. Catal.* **2020**, *41*, 550–560. [CrossRef]
4. Pelalak, R.; Hassani, A.; Heidari, Z.; Zhou, M. State-of-the-art recent applications of layered double hydroxides (LDHs) material in Fenton-based oxidation processes for water and wastewater treatment. *Chem. Eng. J.* **2023**, *474*, 145511. [CrossRef]
5. Liang, R.; Du, Y.; Xiao, P.; Cheng, J.; Yuan, S.; Chen, Y.; Yuan, J.; Chen, J. Transition Metal Oxide Electrode Materials for Supercapacitors: A Review of Recent Developments. *Nanomaterials* **2021**, *11*, 1248. [CrossRef]
6. Zhou, D.; Li, P.; Lin, X.; McKinley, A.; Kuang, Y.; Liu, W.; Lin, W.-F.; Sun, X.; Duan, X. Layered double hydroxide-based electrocatalysts for the oxygen evolution reaction: Identification and tailoring of active sites, and superaerophobic nanoarray electrode assembly. *Chem. Soc. Rev.* **2021**, *50*, 8790–8817. [CrossRef]
7. Li, L.; Soyhan, I.; Warszawik, E.; van Rijn, P. Layered Double Hydroxides: Recent Progress and Promising Perspectives Toward Biomedical Applications. *Adv. Sci.* **2024**, *11*, 2306035. [CrossRef]

8. Hu, T.; Gu, Z.; Williams, G.R.; Strimaite, M.; Zha, J.; Zhou, Z.; Zhang, X.; Tan, C.; Liang, R. Layered double hydroxide-based nanomaterials for biomedical applications. *Chem. Soc. Rev.* **2022**, *51*, 6126–6176. [CrossRef]
9. Chen, B.-Q.; Xia, H.-Y.; Mende, L.K.; Lee, C.-H.; Wang, S.-B.; Chen, A.-Z.; Xu, Z.-P.; Kankala, R.K. Trends in Layered Double Hydroxides-Based Advanced Nanocomposites: Recent Progress and Latest Advancements. *Adv. Mater.* **2022**, *9*, 2200373. [CrossRef]
10. Feng, J.; He, Y.; Liu, Y.; Du, Y.; Li, D. Supported catalysts based on layered double hydroxides for catalytic oxidation and hydrogenation: General functionality and promising application prospects. *Chem. Soc. Rev.* **2015**, *44*, 5291–5319. [CrossRef]
11. Li, H.; Xiao, Z.; Liu, P.; Wang, H.; Geng, J.; Lei, H.; Zhuo, O. Interfaces and Oxygen Vacancies-Enriched Catalysts Derived from Cu-Mn-Al Hydrotalcite towards High-Efficient Water–Gas Shift Reaction. *Molecules* **2023**, *28*, 1522. [CrossRef] [PubMed]
12. Wang, Q.; O'Hare, D. Recent Advances in the Synthesis and Application of Layered Double Hydroxide (LDH) Nanosheets. *Chem. Rev.* **2012**, *112*, 4124–4155. [CrossRef] [PubMed]
13. Zhang, Q.; Shi, X.; Wang, L.; Li, Q.; Xiong, R.; Zhang, Z.; Wu, B.; Yv, C.; Hu, X.; Li, S.; et al. Regulating crystal faces and pore size of layered double oxides for efficient phosphorus recovery from water. *J. Water Process. Eng.* **2025**, *75*, 108033. [CrossRef]
14. Lu, P.; Li, W.; Yang, S.; Wei, Y.; Zhang, Z.; Li, Y. Layered double hydroxides (LDHs) as novel macropore-templates: The importance of porous structures for forward osmosis desalination. *J. Membr. Sci.* **2019**, *585*, 175–183. [CrossRef]
15. Pahalagedara, M.N.; Pahalagedara, L.R.; Kuo, C.-H.; Dharmarathna, S.; Suib, S.L. Ordered Mesoporous Mixed Metal Oxides: Remarkable Effect of Pore Size on Catalytic Activity. *Langmuir* **2014**, *30*, 8228–8237. [CrossRef]
16. Rabe, A.; Jaugstetter, M.; Hiege, F.; Cosanne, N.; Ortega, K.F.; Linnemann, J.; Tschulik, K.; Behrens, M. Tailoring Pore Size and Catalytic Activity in Cobalt Iron Layered Double Hydroxides and Spinels by Microemulsion-Assisted pH-Controlled Co-Precipitation. *ChemSusChem* **2023**, *16*, e202202015. [CrossRef]
17. Wang, A.; Ma, Y.; Zhao, D. Pore engineering of Porous Materials: Effects and Applications. *ACS Nano* **2024**, *18*, 22829–22854. [CrossRef]
18. Wu, F.; Bai, J.; Feng, J.; Xiong, S. Porous mixed metal oxides: Design, formation mechanism, and application in lithium-ion batteries. *Nanoscale* **2015**, *7*, 17211–17230. [CrossRef]
19. Duan, M.; Liu, S.; Jiang, Q.; Guo, X.; Zhang, J.; Xiong, S. Recent progress on preparation and applications of layered double hydroxides. *Chin. Chem. Lett.* **2022**, *33*, 4428–4436. [CrossRef]
20. Prevot, V.; Tokudome, Y. 3D hierarchical and porous layered double hydroxide structures: An overview of synthesis methods and applications. *J. Mater. Sci.* **2017**, *52*, 11229–11250. [CrossRef]
21. Kohay, H.; Gazit, O.M. Regulating adsorption-desorption through controlled modification of the 2D pores in layered double hydroxides. *Surf. Interfaces* **2024**, *44*, 103810. [CrossRef]
22. Jung, S.-Y.; Kim, B.-K.; Hirata, S.; Inada, M.; Oh, J.-M. Particle size effect of layered double hydroxide on the porosity of calcined metal oxide. *Appl. Clay Sci.* **2020**, *195*, 105701. [CrossRef]
23. Oka, Y.; Kuroda, Y.; Matsuno, T.; Kamata, K.; Wada, H.; Shimojima, A.; Kuroda, K. Preparation of Mesoporous Basic Oxides through Assembly of Monodispersed Mg–Al Layered Double Hydroxide Nanoparticles. *Chem. A Eur. J.* **2017**, *23*, 9362–9368. [CrossRef]
24. Guo, C.; Xu, Y.; Ni, C.; Pan, X.; Tijing, L.D.; Shon, H.K.; Deng, N.; Huang, X. Tailoring pore size to enhance dissolution of layered double oxides for efficient nitrogen and phosphorus recovery via crystallization of struvite from wastewater. *J. Colloid Interface Sci.* **2025**, *692*, 137546. [CrossRef]
25. Kim, N.; Gu, T.-H.; Shin, D.; Jin, X.; Shin, H.; Kim, M.G.; Kim, H.; Hwang, S.-J. Lattice Engineering to Simultaneously Control the Defect/Stacking Structures of Layered Double Hydroxide Nanosheets to Optimize Their Energy Functionalities. *ACS Nano* **2021**, *15*, 8306–8318. [CrossRef]
26. Veerabhadrappa, M.G.; Maroto-Valer, M.M.; Chen, Y.; Garcia, S. Layered Double Hydroxides-Based Mixed Metal Oxides: Development of Novel Structured Sorbents for CO_2 Capture Applications. *Acs Appl. Mater. Interfaces* **2021**, *13*, 11805–11813. [CrossRef]
27. Wang, Q.; Chen, L.; Guan, S.; Zhang, X.; Wang, B.; Cao, X.; Yu, Z.; He, Y.; Evans, D.G.; Feng, J.; et al. Ultrathin and Vacancy-Rich CoAl-Layered Double Hydroxide/Graphite Oxide Catalysts: Promotional Effect of Cobalt Vacancies and Oxygen Vacancies in Alcohol Oxidation. *ACS Catal.* **2018**, *8*, 3104–3115. [CrossRef]
28. Liu, S.; Hu, Y.; Zhang, Q.; Tan, X.; Cui, H.; Li, F.; Lei, H.; Zhuo, O. Synthesis of Well-Crystallized Cu-Rich Layered Double Hydroxides and Improved Catalytic Performances for Water–Gas Shift Reaction. *Catalysts* **2025**, *15*, 546. [CrossRef]
29. Zhang, J.; Xie, J.-F.; Yang, J.-C.E.; Li, D.; Zhong, L.-B.; Zheng, Y.-M. Ultra-fast degradation of ciprofloxacin by the peroxymonosulfate activation using a Co/Al-LDH decorated magnetic hydrochar: Structural design, catalytic performance and synergistic effects. *Chem. Eng. J.* **2023**, *477*, 146961. [CrossRef]
30. Tichit, D.; Layrac, G.; Alvarez, M.G.; Marcu, I.-C. Formation pathways of MII/MIII layered double hydroxides: A review. *Appl. Clay Sci.* **2024**, *248*, 107234. [CrossRef]

31. Tathod, A.P.; Gazit, O.M. Fundamental Insights into the Nucleation and Growth of Mg–Al Layered Double Hydroxides Nanoparticles at Low Temperature. *Cryst. Growth Des.* **2016**, *16*, 6709–6713. [CrossRef]
32. Martín, A.J.; Mitchell, S.; Mondelli, C.; Jaydev, S.; Pérez-Ramírez, J. Unifying views on catalyst deactivation. *Nat. Catal.* **2022**, *5*, 854–866. [CrossRef]
33. Kanagaraj, B.; Anand, N.; Raj, R.S.; Lubloy, E. Performance evaluation on engineering properties of sodium silicate binder as a precursor material for the development of cement-free concrete. *Dev. Built Environ.* **2022**, *12*, 100092. [CrossRef]
34. Zhang, Z.F.; Chen, H.; Wang, Y.Q.; Wang, G.; Li, L.H.; Zhong, M.; Bai, H. Effect of sodium silicate binder on the performance of ceramic coatings on copper prepared by the slurry method. *Surf. Coat. Technol.* **2022**, *448*, 128868. [CrossRef]

Disclaimer/Publisher's Note: The statements, opinions and data contained in all publications are solely those of the individual author(s) and contributor(s) and not of MDPI and/or the editor(s). MDPI and/or the editor(s) disclaim responsibility for any injury to people or property resulting from any ideas, methods, instructions or products referred to in the content.